Journal of Power Sources 263 (2014) 268–275

Contents lists available at ScienceDirect

Journal of Power Sources

journal homepage: www.elsevier.com/locate/jpowsour

Amphiphilic carbonaceous material-intervened solvothermal synthesis of $LiFePO_4$

Ming-ming Chen [a,b,*], Qian-qian Ma [a,b], Cheng-yang Wang [a,b], Xin Sun [a,b], Li-qun Wang [a,b], Cui Zhang [a,b]

[a] Key Laboratory for Green Chemical Technology of Ministry of Education, School of Chemical Engineering and Technology, Tianjin University, Tianjin 300072, PR China
[b] Synergetic Innovation Center of Chemical Science and Engineering (Tianjin), Tianjin University, Tianjin 300072, PR China

HIGHLIGHTS

- ACM accelerates the formation of plate-like $LiFePO_4$ parallel to the b_{Pnma} axis.
- ACM suppresses the crystal growth of $LiFePO_4$ along the (010) direction.
- Further ACM coating can greatly improve the electrochemical properties of $LiFePO_4$.

ARTICLE INFO

Article history:
Received 18 December 2013
Received in revised form
24 March 2014
Accepted 11 April 2014
Available online 24 April 2014

Keywords:
Lithium-ion batteries
$LiFePO_4$
Crystal orientation
Carbon coating
Electrochemical properties

ABSTRACT

$LiFePO_4$ samples with preferred facets on the *ac* plane were prepared by the solvothermal method with or without well-dispersed amphiphilic carbonaceous material (ACM). The effects of ACM on the particle morphology, crystal orientation and electrochemical reactivity of the prepared $LiFePO_4$ nanoparticles were investigated in detail. ACM serves a dual purpose. One purpose is facilitating the plate-like morphologies of $LiFePO_4$ nanoparticles parallel to the b_{Pnma} axis by decreasing the surface energy of (010) facets of newly created $LiFePO_4$ nuclei. The other purpose is suppressing crystal growth along the [010] direction by adhering onto the (010) surface of $LiFePO_4$ nanoplates. Furthermore, ACM coating was performed and optimized using a carbon coating precursor. The electrochemical properties of the prepared $LiFePO_4$ particles were characterized by cyclic voltammetry (CV) and galvanostatic charge–discharge cycling tests. After the optimized coating of ACM, the ACM-intervened $LiFePO_4$ composite was observed to deliver discharge capacities of 151.3 mAh g^{-1} at 1C and 132.2 mAh g^{-1} at 10C. Even after 1000 cycles at a high rate of 10C, the $LiFePO_4$ cathode could maintain 80% of its initial capacity.

1. Introduction

Olivine $LiFePO_4$ has been intensively studied as a promising cathode material for high-power lithium-ion batteries (LIBs) in electric vehicles (EVs) [1,2]. The material possesses many advantages, such as high theoretical capacity (170 mAh g^{-1}), low cost, environmentally benign constituents, excellent cycle life, safety and thermal stability. Nevertheless, pure-phase $LiFePO_4$ exhibits poor intrinsic electric conductivity (approximately 10^{-10}–10^{-9} S cm^{-1}) and a low Li-ion diffusion coefficient (approximately 1.8×10^{-14} cm^2 S^{-1}) [3], hindering its application in high-rate batteries.

To date, many studies have been carried out to overcome these limitations of $LiFePO_4$, for example, by tailoring the particle size to the nanometer scale using an in situ polymerization restriction method [4] or by changing the temperature and duration of hydrothermal stripping synthesis [5]; optimizing the morphology to exhibit flower-like and walnut-shaped microspheres [6] or three dimensionally ordered macropores [7]; coating the surface with conductive agents such as non-oriented carbon [8], graphene nanosheets [9] or PPy/PEG [10]; and cation doping with Mn [11] or Rh [12]. In addition, the crystal orientation of $LiFePO_4$ particles is also an important characteristic. Because the crystal structure of $LiFePO_4$ is anisotropic, Li-ion diffusion occurs along the *b*-axis (space group *Pnma*) during charge and discharge, and charge transfer occurs mainly on the *ac* plane [13–16]. In this respect, it appears that the controllable synthesis of $LiFePO_4$ with a short *b*-axis length should facilitate Li-ion diffusion and might be an

* Corresponding author. Key Laboratory for Green Chemical Technology of Ministry of Education, School of Chemical Engineering and Technology, Tianjin University, Tianjin 300072, PR China. Tel./fax: +86 22 27890481.
E-mail address: chmm@tju.edu.cn (M.-m. Chen).

http://dx.doi.org/10.1016/j.jpowsour.2014.04.042
0378-7753/

effective way of increasing the rate performance of $LiFePO_4$. In early studies, many methods were adopted to control the crystal orientation of $LiFePO_4$ [16–28]. Nazar et al. [17] reported that the degree of crystal orientation in the (020) direction can be adjusted to some extent by changing the concentration of the Fe precursor. Kanamura and his co-workers [18] reported that weak acidic solutions with pH levels ranging from 4 to 6.5 can lead to the formation of plate-like crystals with large facets in the *ac* plane; the authors also considered that the crystal growth is governed by kinetic factors that tend to reduce the surface energy of the resulting particles. Vittal [22,23], Li [24], He [25], Yuan [26] and Wang [27] all used an ethylene glycol (EG)-based solvothermal method to synthesize $LiFePO_4$ with a designated crystal orientation. He et al. [25] reported that the largest crystallographic facet of $LiFePO_4$ nanoplates as well as the electrochemical performance thereof can be well tuned by modifying the sequence in which the reactants are added in EG. Such $LiFePO_4$ nanoplates with a crystal orientation along the *ac* facet present a superior electrochemical discharge capacity of 148 mAh g^{-1} at 10C.

In fact, regardless of which of the aforementioned methods is used, $LiFePO_4$ growth occurs by crystallization through the liquid–solid interface. Thus, basic physical chemistry principles indicate that a surfactant will affect $LiFePO_4$ crystal growth. In a previous study, we characterized ACM obtained from pitches as an amphiphilic carbonaceous material that has hydrophobic ends composed of polycyclic aromatic hydrocarbon and hydrophilic surface functional groups (−COOH, −OH, $-SO_3H$, $-NO_2$) [29]. In this study, ACM was used as a surfactant by introducing it into the EG-based solvothermal synthesis of $LiFePO_4$ to determine how ACM affects the oriented formation of $LiFePO_4$ and whether ACM can simultaneously act as both a surfactant and carbon coating precursor [30,31]. Furthermore, $LiFePO_4$ samples synthesized by the ACM-intervened method and ACM coating samples were characterized and tested as cathode materials for lithium-ion batteries with respect to their capacity, cycling stability and rate capability.

2. Experiment

2.1. Material synthesis

ACM was prepared from a coal tar pitch using the method reported in a previous study [29]. ACM is hydrophilic and has a carbon content of 50–60% by mass. A $LiFePO_4$ powder was synthesized using $LiOH{\cdot}H_2O$, $FeSO_4{\cdot}7H_2O$ and H_3PO_4 (85 wt%) as the raw materials: 36 mmol $LiOH{\cdot}H_2O$ was transferred into a beaker containing 60 ml of EG, and 12 mmol H_3PO_4 was subsequently added dropwise into the solution under vigorous stirring. After 0.5 h, 12 mmol $FeSO_4{\cdot}7H_2O$ and ACM (10 wt% of the theoretical mass of $LiFePO_4$) was added to the mixture, which was then continuously stirred for another 0.5 h. The mixture was transferred into a Teflon-lined stainless-steel autoclave and maintained at 180 °C for 10 h. After cooling naturally to room temperature (approximately 25 °C), the resulting precipitate was centrifuged and washed with distilled water till the washing solution became clear and colorless. The precipitate was dried in vacuum at 80 °C for 6 h, and finally, ACM-intervened $LiFePO_4$ was obtained and denoted LFP-ACM.

The carbon coating of LFP-ACM was performed as follows: different concentrations of (0%, 5%, 10% and 15%) ACM were added to a mixture of water and LFP-ACM. The suspensions were ultrasonicated for 0.5 h and subsequently dried in a vacuum oven at 80 °C for 12 h. The dried powder was further heated at 650 °C for 3 h in a tube furnace under a N_2 atmosphere. The final $LiFePO_4$ carbon composites were denoted LFP/C, LFP/C-5, LFP/C-10 and LFP/C-15, respectively.

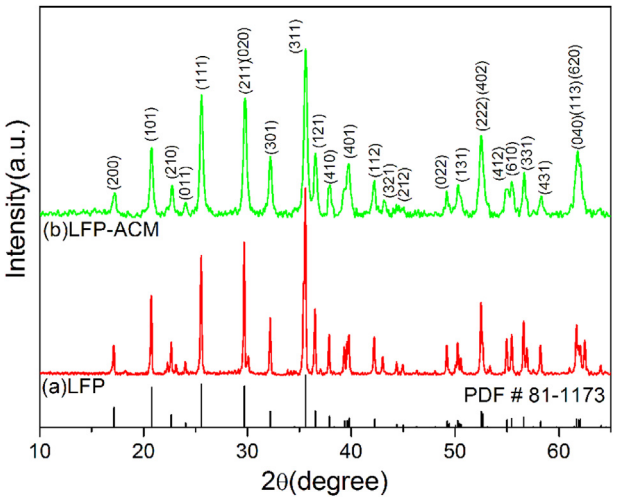

Fig. 1. XRD patterns of (a) LFP and (b) LFP-ACM before heat treatment.

For comparison, LFP refers to the $LiFePO_4$ sample synthesized by the abovementioned method without ACM.

2.2. Carbon content characterization

The practical carbon contents of the samples were determined by the hydrochloric acid dissolution method. First, the samples were added to a 0.1 mol L^{-1} solution of HCl to dissolve $LiFePO_4$. After 0.5 h of magnetic stirring, $LiFePO_4$ was completely dissolved, and the remaining carbon suspension was centrifuged and washed. After drying in 80 °C for 12 h, the residual carbon was weighed, and the carbon contents of the samples were calculated.

2.3. Structural characterization and surface tension test

X-ray diffraction (XRD, Rigaku D/Max-2500V/PC, Rigaku) analysis, performed using Cu Kα radiation (λ = 1.5406 Å) over a scanning range of 10°–80° at 4° min^{-1}, was used to identify the crystalline phases of the prepared samples. The lattice parameters were determined by whole-pattern refinement using Rietveld refinement software (MDI). The morphology and structure of the samples were analyzed via field-emission scanning electron microscopy (FESEM, Nano430, America) and high-resolution transmission electron microscopy (HRTEM, Tecnai G2F20, Philips). The surface tensions of the samples were measured by pendant drop experiments using an automated drop tensiometer (the Tracker, Teclis, France).

2.4. Electrochemical measurements

The electrochemical performance of the cathode materials was characterized by using a CR2430 coin cell and lithium counter electrode. Composite electrodes were fabricated by combining the active material, acetylene black and poly(vinylidene fluoride) (PVDF) binder in a weight ratio of 80:10:10 using *N*-methyl-2-pyrrolidone (NMP) as a solvent to form a homogeneous slurry. Subsequently, the slurry was coated onto an Al foil and dried in a vacuum oven at 120 °C for 12 h; the foil was then cut into discs, which were used as working electrodes. The loading of the active materials on the working electrodes was approximately 2 mg cm^{-2}. A mixture composed of 1 M $LiPF_6$ and ethylene carbonate (EC)/diethyl carbonate (DEC) (1:1 in volume) and a Celgard 2400 membrane were used as the electrolyte and separator, respectively. Galvanostatic charge–discharge cycling tests of the assembled cells

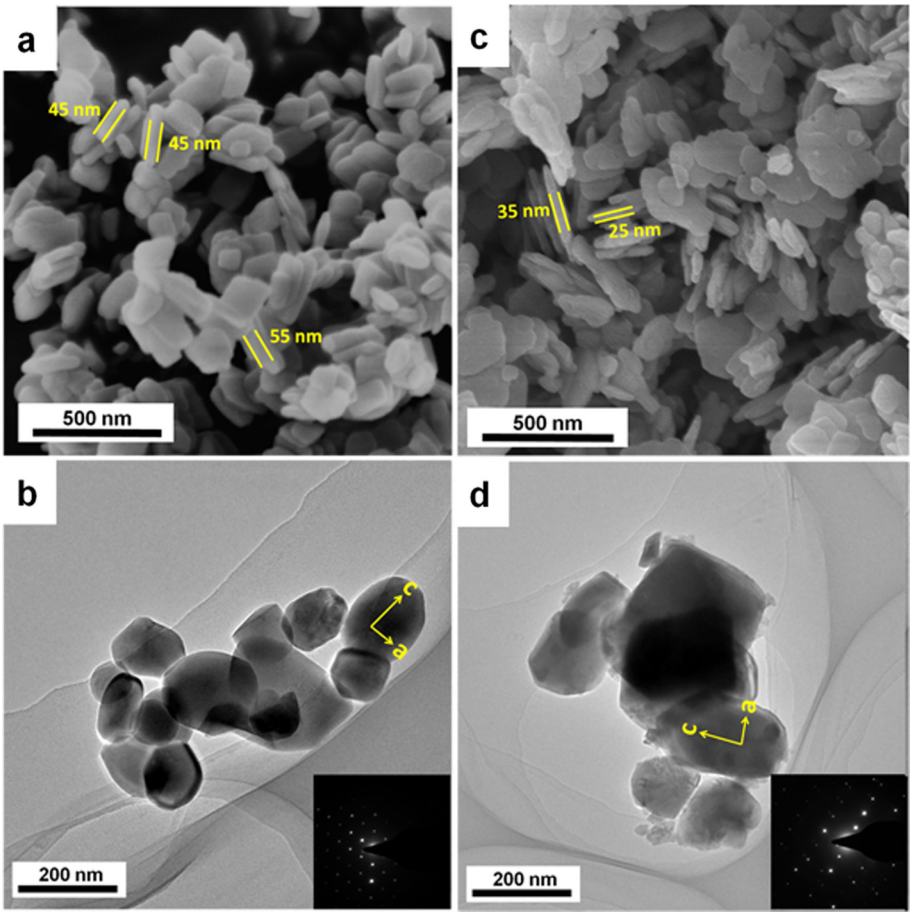

Fig. 2. FESEM and TEM images (SEAD inside) of (a–b) LFP and (c–d) LFP-ACM before heat treatment.

were performed on an electrochemical test instrument (CT2001A, Wuhan Land Electronic Co. Ltd., China) at various current rates over a voltage range of 2.0–4.2 V (*vs.* Li/Li^+, 1C = 170 mAh g^{-1}) at room temperature (25 °C). Cyclic voltammetry (CV) was performed from 2.5 to 4.2 V (*vs.* Li/Li^+) using a Princeton Parstant 2273 electrochemical system.

3. Results and discussion

Fig. 1 shows the XRD patterns of the two $LiFePO_4$ samples solvothermally synthesized with ACM (LFP-ACM) and without ACM (LFP). The two patterns exhibit the same major peaks and match the pattern of standard crystallized orthorhombic $LiFePO_4$ well (PDF No. 81-1173, space group *Pnma*), suggesting perfect crystallinity without impurities. The lattice parameters for the LFP sample synthesized in the absence of ACM were measured to be a = 10.327 Å, b = 6.010 Å and c = 4.698 Å, whereas values of a = 10.322 Å, b = 6.008 Å and c = 4.670 Å were observed for the LFP-ACM sample. Both sets of crystal lattice parameters are very similar to the values indicated by PDF No. 81-1173 (a = 10.332 Å, b = 6.010 Å and c = 4.692 Å). Moreover, the lattice parameters did not show significant changes with the addition of ACM.

In Kanamura's [18] and He's publications [25] concerning $LiFePO_4$, the XRD peak intensity ratio of $I_{(020)}/I_{(200)}$ was referred to as a benchmark for $LiFePO_4$ crystal orientation. Kanamura et al. [18] suggested that if the ratio of $I_{(020)}/I_{(200)}$ is greater than that of the standard (PDF No. 81-1173), platelet-type structures with a preferential growth direction along the *ac* facet would be observed. In fact, the $I_{(020)}/I_{(200)}$ ratio of PDF-81-1173 is 2.1 [25]. In Fig. 1a and b, the $I_{(020)}/I_{(200)}$ ratios are shown to be 4.4 for the LFP sample and 4.9 for the LFP-ACM sample. That is, regardless of whether ACM was added, the exposed facets were mostly *ac* facets for both the LFP and LFP-ACM samples. However, the $I_{(020)}/I_{(200)}$ ratio of LFP-ACM is higher than that of LFP, suggesting that the addition of ACM in the solvothermal process facilitates preferential crystal growth along the *ac* facet and the LFP-ACM sample exhibits a higher degree of crystal orientation than the LFP sample. The reasons for these observations are discussed in detail in the following section.

To further confirm the preferred crystal growth orientations and observe the crystals formed by the different samples, FESEM and HRTEM measurements were performed. Fig. 2 shows FESEM and TEM images of the LFP and LFP-ACM samples obtained after undergoing solvothermal reaction for 10 h. It can be clearly observed from Fig. 2a and c that both samples are mainly composed of nanoplates measuring 90–250 nm, but the thickness of LFP-ACM (25–35 nm) is smaller than that of LFP (45–55 nm). Further observation by TEM and SAED (selected area electron diffraction) (Fig. 2b and d) revealed that the nanoplates of both LFP and LFP-ACM are single crystals with the *b*-axis lying along the thin direction and the large face of the nanoplates lying in the *ac* plane. This result is similar to that reported by Nan et al. [24] and other authors [25–27] who also used EG as the solvent. These authors considered that EG acts not only as a solvent but also as a soft template for the crystal growth of $LiFePO_4$ along the (010) facet due to its special chelating ability. Moreover, the nanoplates of LFP-ACM are thinner than those of LFP, mainly due to the addition of ACM during the solvothermal process.

To understand the formation of the $LiFePO_4$ nanoplate structures in the ACM-intervened EG solution, time-dependent

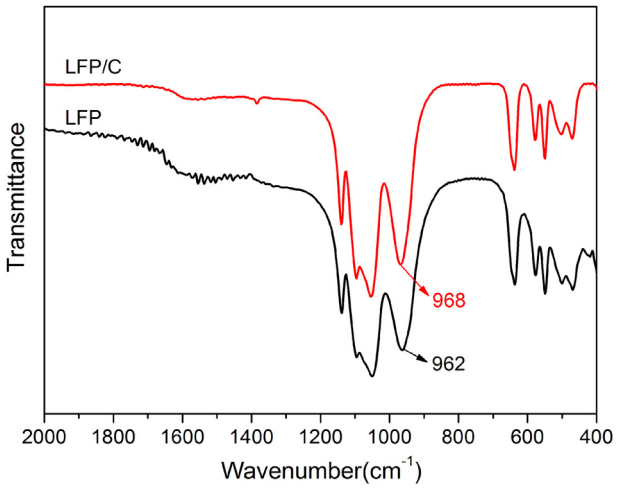

Fig. 3. Fourier transform infrared spectroscopy (FTIR) spectra of LFP and LFP/C samples.

experiments were conducted. The XRD pattern of the 0-h sample (Fig. 1S) indicates the formation of the Li_3PO_4 phase immediately before transferring it to the hydrothermal autoclave. Solvothermal treatment at 180 °C for 1 h generated a noticeable change in the XRD pattern (Fig. 1S). The diffraction peaks of Li_3PO_4 nearly disappeared, and $LiFePO_4$ could be properly indexed. Fig. 2S(b) shows that the 1-h sample was mainly composed of nanoparticles measuring 10–15 nm. With an increase in the reaction time from 4 h to 7 h, the peaks of $LiFePO_4$ became strong and narrow (see the XRD patterns in Fig. 1S), suggesting improved crystallinity. Many nanoplates measuring 50–60 nm could be observed after 4 h of solvothermal treatment (Fig. 2S(c)), which suggests that the $LiFePO_4$ nuclei had already begun to grow and evolve into nanoplates. When the reaction time was extended to 7 h, nanoplates measuring 90–200 nm were formed.

The results above show that ACM and the reaction medium play the important roles in the formation of the $LiFePO_4$ nanoplates. First, EG causes $LiFePO_4$ particles to appear as nanoplates with a (010) facet orientation [24–27]. Next, we must consider the properties of ACM. ACM is obtained by harsh oxidation from coal tar pitch, which is a mixture of polycyclic aromatic hydrocarbons (PAHs). At the edge of the PAHs, many surface functional groups such as −COOH, −OH, $-SO_3H$ and $-NO_2$ are introduced [29], making ACM an aromatic compound that facilitates nucleophilic addition and nucleophilic substitution. That is, the hydrophobic ends that are composed of PAHs are slightly positively charged (δ^+) due to the electron-withdrawing inductive effect. On the other hand, when tiny $LiFePO_4$ plates are newly created in the EG solution, the top layers of the plates are negatively charged, based on Islam's calculation [33], such that the outer layer of (010) facets intrinsically contains 50% Li vacancies relative to the bulk. Thus, the outer layer will most certainly be affected by the positively charged hydrophobic end of ACM. ACM may adhere to the (010) surface of the nanoplates, making the ACM-terminated (010) surfaces more stable and further suppressing crystal growth along the (010) direction. Therefore, with the help of ACM, the LFP-ACM sample grows more slowly along the *b*-axis direction than the LFP sample and yields thinner nanoplates.

In addition, according to Islam's atomic-scale simulation concerning the morphology of crystal $LiFePO_4$ [33] and Wang's report [27] on the thermodynamic control of morphology by surface energy, the thinness of the plate-like morphologies parallel to the b_{Pnma} axis requires the (010) surface to be significantly lower in

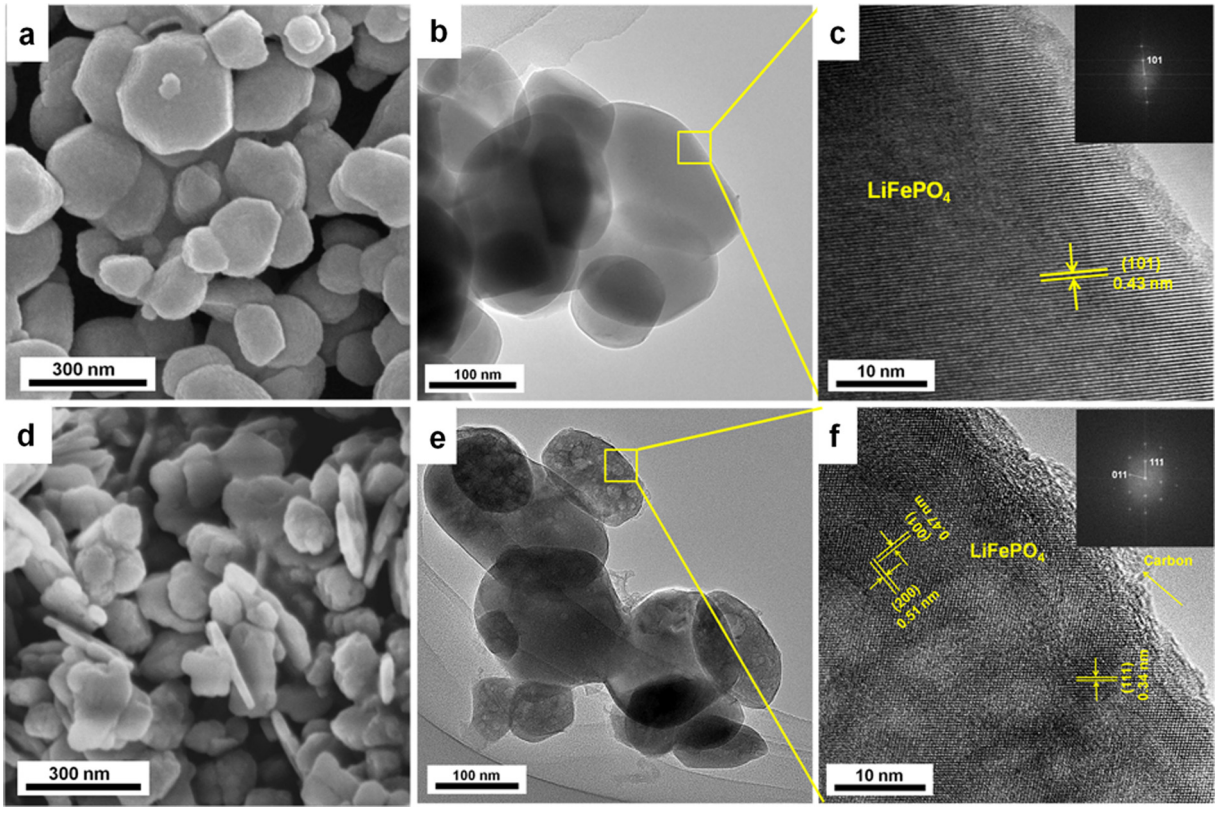

Fig. 4. FESEM and TEM images (FFT inside) of (a–c) LFP and (d–f) LFP/C after heat treatment at 650 °C.

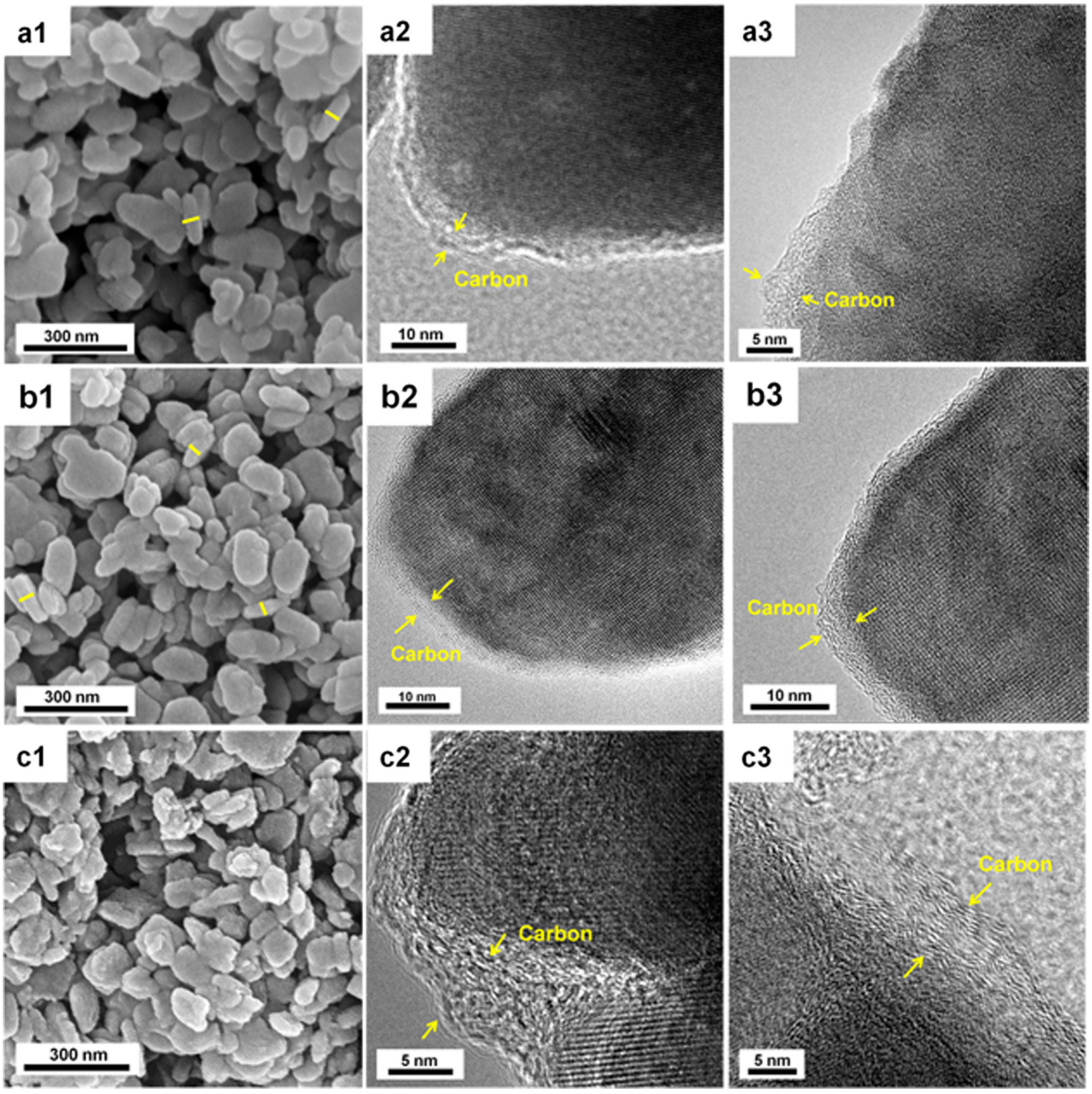

Fig. 5. FESEM and HRTEM images of (a1–a3) LFP/C-5, (b1–b3) LFP/C-10 and (c1–c3) LFP/C-15.

energy than the other surfaces. ACM can be regarded as a surfactant due to its hydrophilic head and hydrophobic end. In fact, the surface tension of the EG solution was reduced from 45.18 mN m^{-1} without ACM to 41.08 mN m^{-1} after adding ACM. Although it is not a typical surfactant, ACM affects the surface energy of the EG solution to a certain extent. It is assumed that the surface energy of the *ac* plane is lower than that of other crystal planes under EG-based solvothermal conditions [34], and the addition of ACM to the solution can further decrease the surface energy of the *ac* plane. Thus, it can be concluded that the interaction between ACM and EG facilitates $LiFePO_4$ plate growth along the *ac* facets and helps yield a higher ratio of $I_{(020)}/I_{(200)}$.

Because Li ions move through the tunnels along the *b*-axis in $LiFePO_4$, Li-ion migration is determined not only by particle size and available diffusion pathways but is also significantly affected when the channels are blocked by defects created during $LiFePO_4$ formation. The $Fe^{\$}_{Li}$ antisite defects in the LFP and LFP/C samples were characterized by FTIR. In the FTIR spectrum, the adsorption band of the P–O symmetric stretching vibration (including defects) occurs at approximately 1000 cm^{-1}, whereas that of defect-free $LiFePO_4$ is located at 957 cm^{-1} [25,27]. In Fig. 3, the P–O symmetric stretching vibrations are located at 962 and 968 cm^{-1} for LFP and LFP/C, respectively, implying that the defect concentrations of the $Fe^{\$}_{Li}$ antisite in the two samples are very low, which benefits

Table 1
The carbon content of the samples.

Sample	ACM used (wt%)	Carbon content after 650 °C heat-treatment (wt%)
LFP/C	10[a]	1.1
LFP/C-5	5[b]	3.8
LFP/C-10	10[b]	6.8
LFP/C-15	15[b]	9.5

[a] The amount of ACM used was 10 wt% of the theoretical mass of LFP.
[b] The concentration of ACM used was calculated as the mass of ACM added divided by the total mass of LFP-ACM.

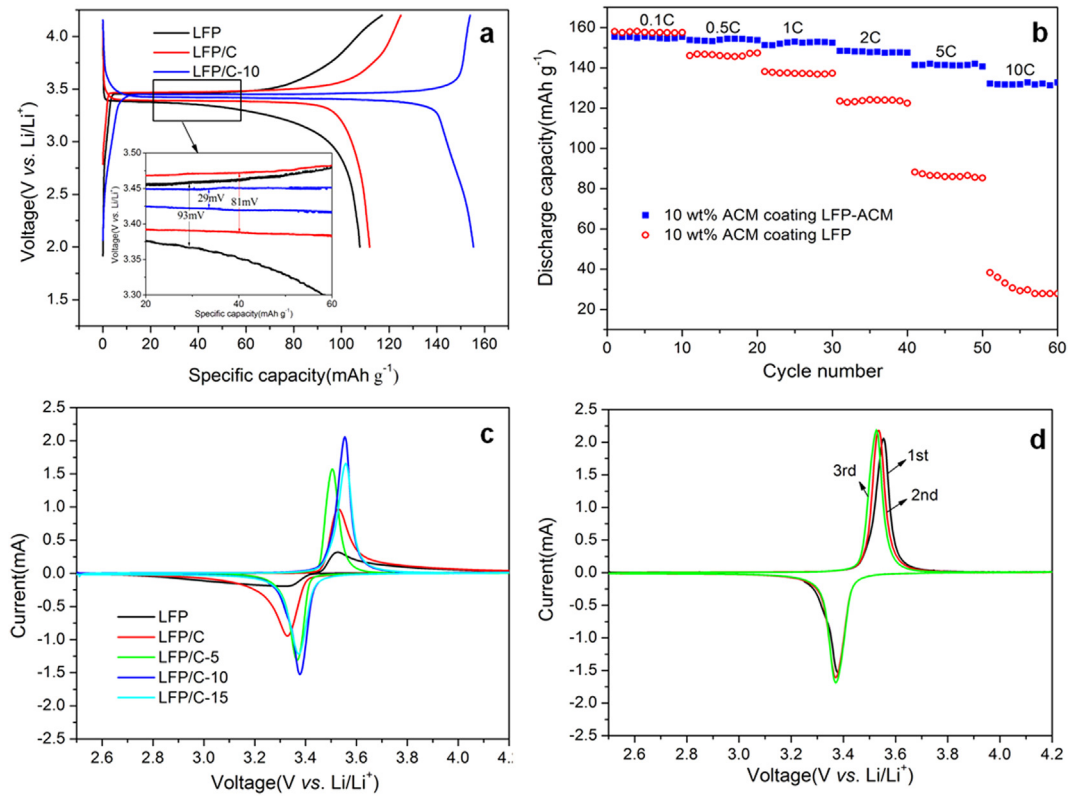

Fig. 6. (a) First charge–discharge curves for the sample electrodes at a rate of 0.1C; the inset shows a magnification of the flat regions. (b) Comparison of C-rate capability between LFP sample and LFP-ACM sample coated with 10 wt% ACM coating (from 0.1C to 10C). (c) Cyclic voltammograms of the samples LFP, LFP/C, LFP/C-5, LFP/C-10 and LFP/C-15 obtained at a scan rate of 0.1 mV s^{-1}. (d) CV profiles of LFP/C-10 over the first three charge–discharge cycles at 0.1 mV s^{-1} between 2.5 and 4.2 V.

Li-ion migration. The result also indicates that the addition of ACM during EG-based solvothermal synthesis does not increase the concentration of $Fe_{Li}^{\$}$ antisite defects.

After heat treatment at 650 °C, the preferred crystal orientation of LFP and LFP/C is still along the *b*-axis (Fig. 4c and f), but the ratios of $I_{(020)}/I_{(200)}$ for the samples decreases to 3.2 and 3.8 (Fig. 3S), respectively. This decrease may be due to agglomeration during high-temperature heat treatment, as shown in Fig. 4a and d. However, some LFP/C particles retain their plate-like morphology (Fig. 4d). It is speculated that carbon residue (which is formed by the carbonization of ACM) remaining on the surface of the particles (see Fig. 4e and f) suppresses nanoplate agglomeration. When the LFP and LFP/C nanoplates were further coated with ACM, the agglomeration phenomenon could not be observed (Fig. 4S and Fig. 5(a1)–(c1)).

The Li-ion diffusion coefficient is the most important factor affecting electrode kinetics [35]. Based on the Randles–Sevcik equation [36] and the cyclic voltammograms (CVs) of LFP and LFP/C (Fig. 5S(a) and (b)) obtained at scan rates ranging from 0.1 mV s^{-1} to 1.5 mV s^{-1}, the apparent diffusion coefficient of Li-ion ($D_{Li^+}^{app}$) in each sample was calculated. The values of $D_{Li^+}^{app}$ for LFP and LFP/C were calculated to be 3.56×10^{-12} and 3.45×10^{-10} cm^2 s^{-1}, respectively. These data indicate that the LFP/C particles possessed a Li-ion apparent diffusion coefficient that was two orders of magnitude greater than that of the LFP particles.

Fig. 4f shows that ACM could not act as an in situ carbon coating precursor. Owing to its hydrophilicity, ACM adhered to the outermost surface of the particles was partially washed off during subsequent washing. Nevertheless, trace carbon residue (1.1 wt%, in Table 1) thermochemically converted from ACM at 650 °C provided a partial improvement in the electric conductivity (discussed later) of the whole material. Of course, as an electrode material, LFP/C requires further improvements in its electric conductivity, for example, by carbon coating.

ACM was again used as a carbon coating precursor. It was observed that 10 wt% ACM was the optimal concentration. At 5 wt% ACM, not all of the LFP/C surfaces were covered by carbon (Fig. 5(a1)–(a3)), whereas 15 wt% ACM caused the electrode materials to be over-coated (Fig. 5(c1)–(c3)). The TEM images shown in Fig. 5(b2)–(b3) illustrate that the LFP/C-10 sample surface was coated by a continuous and amorphous carbon layer measuring 2–3 nm in thickness. Although the amount of ACM used was approximately 10 wt%, the residual carbon remaining after heat treating the sample at 650 °C was only 6.8 wt% (in Table 1) because of the runoff of non-carbon atoms in ACM during the heat treatment. The surface of LFP/C-10 was smooth, and a core–shell structure was formed. The carbon shell formed a network connecting individual $LiFePO_4$ nanoparticles, effectively providing conductive pathways and improving the electrochemical performance of the LFP/C-10 composite.

The electrochemical properties of the samples were investigated. Fig. 6a compares the initial charge–discharge curves of cells based on LFP, LFP/C and LFP/C-10 at 0.1C. The LFP sample shows a very low discharge capacity of only 107.7 mAh g^{-1}. The value of ΔE (93 mV), the difference between the charge and discharge potential, illustrates the high extent of the composite's polarization. The LFP/C sample comparatively shows an improved discharge capacity of 111.8 mAh g^{-1}, a lengthened voltage plateau and a reduced ΔE value of 81 mV. All of these improvements are attributed to the fact that the structure of the LFP/C sample is more beneficial for Li-ion migration and higher conductivity is afforded by the carbon residue from ACM. It is noted that the coated sample LFP/C-10 exhibited the

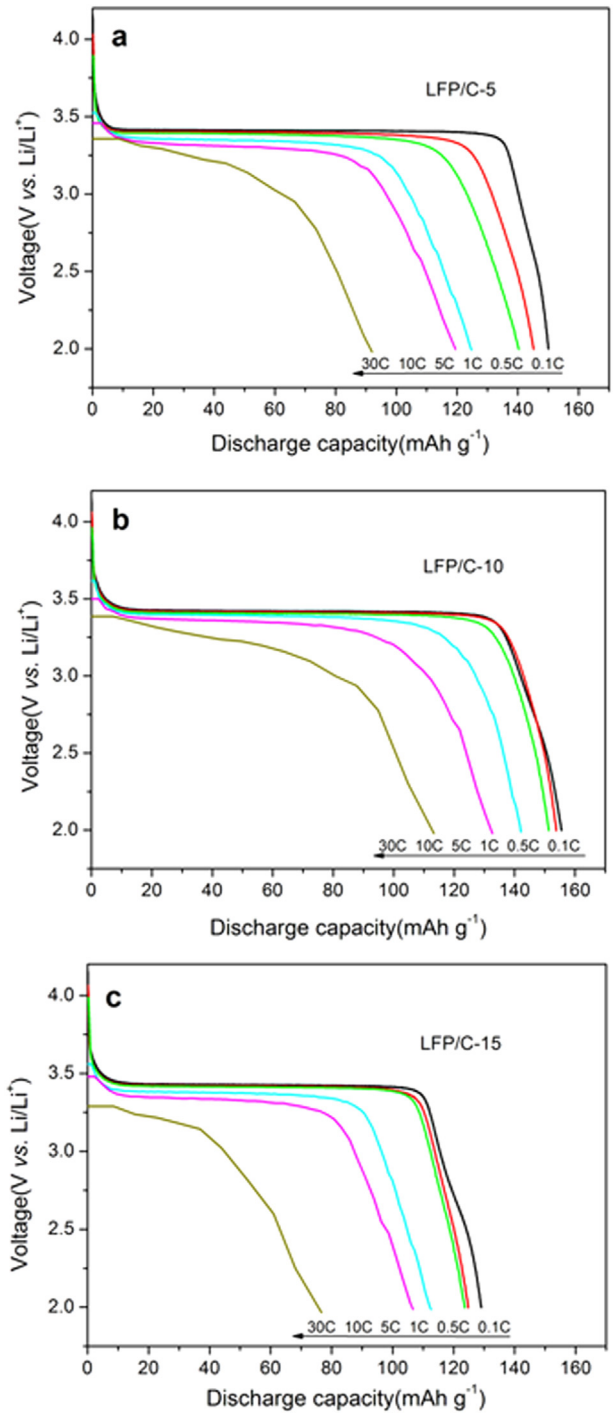

Fig. 7. Discharge curves for (a) LFP/C-5, (b) LFP/C-10 and (c) LFP/C-15 obtained at different rates (from 0.1C to 30C).

best performance. The discharge capacity of this sample was 155.4 mAh g^{-1}, and the sample showed a highly reduced ΔE value of only 29 mV. The high capacity and low ΔE of the LFP/C-10 cathode are believed to be related to not only the continuous carbon-coating layer but also the plate-like morphology of $LiFePO_4$ parallel to the *b*-axis. In reality, the morphology of LFP-ACM is more important. The importance of the composite's morphology is also indicated by the results shown in Fig. 6b. Although both the LFP and LFP-ACM samples were further carbon coated by the addition of 10 wt% ACM, when a current rate of 1C or above was applied, the former presented a more rapid decay in capacity compared to the latter.

Fig. 6c shows the first-round CVs of the samples LFP, LFP/C, LFP/C-5, LFP/C-10 and LFP/C-15 obtained between 2.5 and 4.2 V at a scan rate of 0.1 mV s^{-1}. A few anodic and cathodic peaks in the range of 3.30–3.60 V correspond to the two-dimensional charge–discharge reaction between $LiFePO_4$ and $FePO_4$. A comparison of the LFP/C and LFP samples reveals that the former shows a pair of symmetrical redox peaks of approximately equal peak area, but the latter does not. This finding suggests that LFP/C exhibits good Li-ion insertion/extraction reversibility. The LFP/C-5, LFP/C-10 and LFP/C-15 samples all present sharp anodic/cathodic CV peaks and narrow peak-to-peak separation. Based on the CV of the LFP/C cathode, it is determined that even though the LFP/C sample possesses a well-defined orientation along the (010) direction, an optimum carbon coating is still needed to overcome the low electronic conductivity of the $LiFePO_4$ particles.

Among all three carbon-coated cathodes, i.e., LFP/C-5, LFP/C-10 and LFP/C-15, the sharpest CV peaks were observed for the LFP/C-10 electrode (Fig. 6c). Moreover, as demonstrated by the first three CV curves of LFP/C-10 obtained at a scan rate of 0.1 mV s^{-1} in Fig. 6d, the second and third cycles are nearly superimposed on one another, indicating that excellent electrochemical reversibility was established for the LFP/C-10 cathode after the initial charge–discharge cycle. A comparison of the discharge curves of the carbon-coated samples obtained at different rates, shown in Fig. 7a–c, reveals that the LFP/C-10 sample showed the best performance. Overall, these electrochemical data indicate that the LFP/C-10 composite exhibits high electrochemical reactivity, small polarization, a high Li-ion diffusion rate and low inner resistance.

Furthermore, the LFP/C-10 cathode also exhibits satisfactory cycling stability and rate capability under high-rate, long-term operation. Fig. 8a shows the Li-ion intercalation capacity of LFP/C and the carbon-coated composite electrodes at different rates, first from 0.1C to 60C and then back to 0.1C. All of the samples were cycled 10 times at each rate and then forwarded to the next step. Among the samples, LFP/C-10 delivered discharge capacities of 155.4, 151.3, 141.4 and 132.2 mAh g^{-1} at 0.1C, 1C, 5C and 10C, respectively. When the current density was increased to 30C and 60C, the discharge capacity (at 113.3 and 93.5 mAh g^{-1}, respectively) remained relatively high, demonstrating 73% and 60% capacity retention compared to the capacity at 0.1C. When the current rate was returned to 0.1C after cycling at 60C, the discharge capacity rebounded to 146.9 mAh g^{-1}, representing only a 5.5% decay relative to the original capacity. The LFP/C-10 cathode did not decay after 100 cycles at 1C, 5C and 10C (shown in the inset of Fig. 8b). Even after 1000 cycles at 10C (Fig. 8b), the LFP/C-10 cathode still retained 80% of its initial capacity (132.2 mAh g^{-1}), and the coulombic efficiency was always near 100% throughout the entire cycling process.

4. Conclusions

$LiFePO_4$ samples with a plate-like morphology parallel to the b_{Pnma} axis were prepared by the ACM-intervened ethylene glycol-based solvothermal method at 180 °C using a Li:Fe:P mole ratio of 3:1:1. The addition of ACM does not increase the concentration $Fe^{\$}_{Li}$ antisite defects but does induce the formation of plate-like morphologies parallel to the b_{Pnma} axis by successfully decreasing the surface energy of (010) facets of newly created $LiFePO_4$ nuclei. Conversely, ACM suppresses crystal growth along the (010) direction by adhering to the (010) surfaces of $LiFePO_4$ nanoplates. After carbon coating with 10 wt% ACM, the composite samples were observed to deliver discharge capacities of 151.3 mAh g^{-1} at 1C and 132.2 mAh g^{-1} at 10C. Even after 1000 cycles at a high rate of 10C,

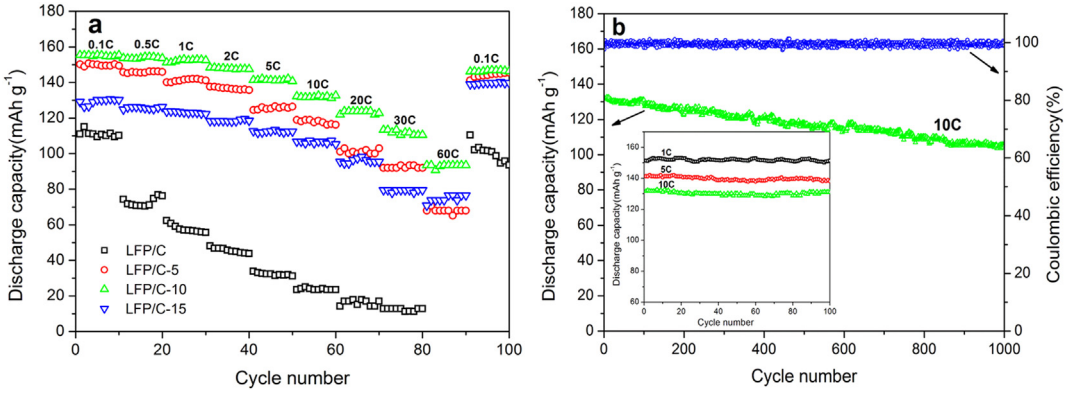

Fig. 8. (a) Lithium-ion intercalation capacities of LFP/C, LFP/C-5, LFP/C-10 and LFP/C-15 composite electrodes at different discharge rates ranging from 0.1C to 60C. (b) Long-term stability of LFP/C-10 cathode at high current rates.

the carbon-coated oriented $LiFePO_4$ cathode could still maintain 80% of its initial capacity.

Acknowledgments

The author would like to thank Prof. Hong-lai Liu for his help in performing the surface tension tests and useful discussion about surfactants.

This work was supported by the National Natural Science Foundation of China (NSFC 51372168) and the Natural Science Foundation of Tianjin City of China (Key program, No. 12JCZDJC27000).

Appendix A. Supplementary data

Supplementary data related to this article can be found at http://dx.doi.org/10.1016/j.jpowsour.2014.04.042.

References

[1] A.K. Padhi, K.S. Nanjundaswamy, J.B. Goodenough, J. Electrochem. Soc. 144 (1997) 1188.
[2] B. Scrosati, Electrochim. Acta 45 (2000) 2461–2466.
[3] P.P. Prosini, M. Lisi, D. Zane, M. Pasquali, Solid State Ionics 148 (2002) 45–51.
[4] Y.G. Wang, Y.R. Wang, E. Hosono, K.X. Wang, H.S. Zhou, Angew. Chem. Int. Ed. 47 (2008) 7461–7465.
[5] X.Y. Wang, C. Miao, J. Zhou, C. Ma, H.F. Wang, S.Q. Sun, Mater. Lett. 65 (2011) 2096–2099.
[6] C.W. Sun, S. Rajasekhara, J.B. Goodenough, F. Zhou, J. Am. Chem. Soc. 133 (2011) 2132–2135.
[7] C.H. Yim, E.A. Baranova, Y. Abu-Lebdeh, I. Davidson, J. Power Sources 205 (2012) 414–419.
[8] N. Zhou, E. Uchaker, Y.Y. Liu, S.Q. Liu, Y.N. Liu, G.Z. Cao, Int. J. Electrochem. Sci. 7 (2012) 12633–12645.
[9] C. Su, X.D. Du, L.H. Xu, J.L. Liu, C. Zhang, Electrochim. Acta 64 (2012) 190–195.
[10] A. Fedorková, R. Oriňáková, A. Oriňák, I. Talian, A. Heile, H.D. Wiemhöfer, D. Kaniansky, H.F. Arlinghaus, J. Power Sources 195 (2010) 3907–3912.
[11] J. Zong, Q.W. Peng, J.P. Yu, X.J. Liu, J. Power Sources 228 (2013) 214–219.
[12] D.G. Tong, F.L. Luo, W. Chu, Y.L. Li, P. Wu, Mater. Chem. Phys. 124 (2010) 1–5.
[13] D. Morgan, A. Van der Ven, G. Ceder, Electrochem. Solid-State Lett. 7 (2004) A30–A32.
[14] M.S. Islam, D.J. Driscoll, C.A.J. Fisher, P.R. Slater, Chem. Mater. 17 (2005) 5085–5092.
[15] R. Amin, P. Balaya, J. Maier, Electrochem. Solid-State Lett. 10 (2007) A13–A16.
[16] D.H. Kim, J. Kim, Electrochem. Solid-State Lett. 9 (2006) A439–A442.
[17] B. Ellis, W.H. Kan, W.R.M. Makahnouk, L.F. Nazar, J. Mater. Chem. 17 (2007) 3248–3254.
[18] K. Dokko, S. Koizumi, H. Nakano, K. Kanamura, J. Mater. Chem. 17 (2007) 4803–4810.
[19] K. kanamura, S. Koizumi, K. Dokko, J. Mater. Sci. 43 (2008) 2138–2142.
[20] S. Ferrari, R.L. Lavall, D. Capsoni, E. Quartarone, A. Magistris, P. Mustarelli, P. Canton, J. Phys. Chem. C 114 (2010) 12598–12603.
[21] S.L. Yang, X.F. Zhou, J.G. Zhang, Z.P. Liu, J. Mater. Chem. 20 (2010) 8086–8091.
[22] K. Saravanan, M.V. Reddy, P. Balaya, H. Gong, B.V.R. Chowdari, J.J. Vittal, J. Mater. Chem. 19 (2009) 605–610.
[23] K. Saravanan, P. Balaya, M.V. Reddy, B.V.R. Chowdari, J.J. Vittal, Energy Environ. Sci. 3 (2010) 457–464.
[24] C.Y. Nan, J. Lu, C. Chen, Q. Peng, Y.D. Li, J. Mater. Chem. 21 (2011) 9994–9996.
[25] L. Wang, X.M. He, W.T. Sun, J.L. Wang, Y.D. Li, S.S. Fan, Nano Lett. 12 (2012) 5632–5636.
[26] M. Wu, Z.H. Wang, L.X. Yuan, W.X. Zhang, X.L. Hu, Y.H. Huang, Chin. Sci. Bull. 57 (2012) 4170–4175.
[27] X. Qin, J.M. Wang, J. Xie, F.Z. Li, L. Wen, X.H. Wang, Phys. Chem. Chem. Phys. 14 (2012) 2669–2677.
[28] X.H. Rui, X.X. Zhao, Z.Y. Lu, H.T. Tan, D.H. Sim, H.H. Hng, R. Yazami, T.M. Lim, Q.Y. Yan, ACS Nano 7 (2013) 5637–5646.
[29] L.Q. Wang, J.Z. Wang, F. Jia, C.Y. Wang, M.M. Chen, J. Mater. Chem. A 1 (2013) 9498–9507.
[30] J. Wang, M.M. Chen, C.Y. Wang, B.Q. Hu, J.M. Zheng, Mater. Lett. 64 (2010) 2281–2283.
[31] X.F. Guo, C.Y. Wang, M.M. Chen, J.Z. Wang, J.M. Zheng, J. Power Sources 214 (2012) 107–112.
[33] C.A.J. Fisher, M.S. Islam, J. Mater. Chem. 18 (2008) 1209–1215.
[34] Z.P. Ma, G.J. Shao, X. Wang, J.J. Song, G.L. Wang, T.T. Liu, Mater. Chem. Phys. 143 (2014) 969–976.
[35] L.X. Li, X.C. Tang, H.T. Liu, Y. Qu, Z.G. Lu, Electrochim. Acta 56 (2010) 995–999.
[36] Y.D. Cho, G.T.K. Fey, H.M. Kao, J. Power Sources 189 (2009) 256–262.